

Is the Dark Halo of the Milky Way Prolate?

A. Bowden^{1*}, N. W. Evans¹, A. A. Williams¹

¹*Institute of Astronomy, University of Cambridge, Madingley Road, Cambridge, CB3 0HA, UK*

Accepted Received ; in original form

ABSTRACT

We introduce *the flattening equation*, which relates the shape of the dark halo to the angular velocity dispersions and the density of a tracer population of stars. It assumes spherical alignment of the velocity dispersion tensor, as seen in the data on stellar halo stars in the Milky Way. The angular anisotropy and gradients in the angular velocity dispersions drive the solutions towards prolateness, whilst the gradient in the stellar density is a competing effect favouring oblateness. We provide an efficient numerical algorithm to integrate the flattening equation. Using tests on mock data, we show that there is a strong degeneracy between circular speed and flattening, which can be circumvented with informative priors. Therefore, we advocate the use of the flattening equation to test for oblateness or prolateness, though the precise value of q can only be measured with the addition of the radial Jeans equation. We apply the flattening equation to a sample extracted from the *Sloan Digital Sky Survey* of ~ 15000 halo stars with full phase space information and errors. We find that between Galactocentric radii of 5 and 10 kpc, the shape of the dark halo is prolate, whilst even mildly oblate models are disfavoured. Strongly oblate models are ruled out. Specifically, for a logarithmic halo model, if the asymptotic circular speed v_0 lies between 210 and 250 kms^{-1} , then we find the axis ratio of the equipotentials q satisfies $1.5 \lesssim q \lesssim 2$.

Key words: Galaxy: halo – Galaxy: kinematics and dynamics – Galaxy: structure

1 INTRODUCTION

The flattening of the Milky Way’s dark halo is a subject of much interest, but also alas much confusion. The flaring of the HI gas layer, the modelling of tidal tails (particularly of the Sagittarius stream) and the kinematics of stars have all been used to determine the shape. The literature contains claims that the dark halo is oblate (Olling & Merrifield 2000; Koposov et al. 2010; Bowden et al. 2015), spherical (Fellhauer et al. 2006; Smith et al. 2009a), prolate (Helmi 2004; Banerjee & Jog 2011) and triaxial (Law & Majewski 2010). Not all of these claims can be correct, even though the flattening could change with radius (e.g., Vera-Ciro & Helmi 2013).

The shape of the dark halo controls the kinematics of stellar halo stars via the Jeans equations. In recent years, there has been a growing consensus that the density of the stellar halo has an oblate double-power law or Sersic profile structure (see e.g., Watkins et al. 2009; Deason et al. 2011; Pila-Díez et al. 2015) with a flattening or axis ratio of q_* ≈ 0.6 . Once the density law is reliably known, the motions of the stellar halo stars enable the gravity field, and hence the shape, of the dark halo to be ascertained.

Data sets with full phase-space information for stars in the smooth inner halo are beginning to become available. The largest to date has been presented by Bond et al. (2010). Halo stars are extracted from the Sloan Digital Sky Survey (SDSS) by combined color and metallicity cuts, whilst SDSS spectroscopy is used for radial velocities and Palomar Observatory Sky Survey (POSS) astrometry for proper motions. This gives a sample of ~ 15000 halo stars with all 6 phase space coordinates.

The Jeans equations are often used in modelling external galaxies for which only projected or line of sight data are usually measurable (e.g., Binney et al. 1990; Cappellari 2008). However, the situation with the stellar halo of the Milky Way is rather different in that line of sight velocities and proper motions are often available. All the components of the stress or velocity dispersion tensor are in principle measurable, as well as their spatial gradients. This motivates new approaches. For example, Loebman et al. (2014) have pioneered a technique in which the data are used to derive acceleration maps throughout the observed volume. By fitting the acceleration maps to models, they find that the dark matter halo is very highly flattened with an axis ratio of $q = 0.4 \pm 0.1$. Here, we shall present another technique which exploits the three dimensional nature of the kinematic data now available for the Milky Way.

* E-mail: adb61,nwe,aamw3@ast.cam.ac.uk

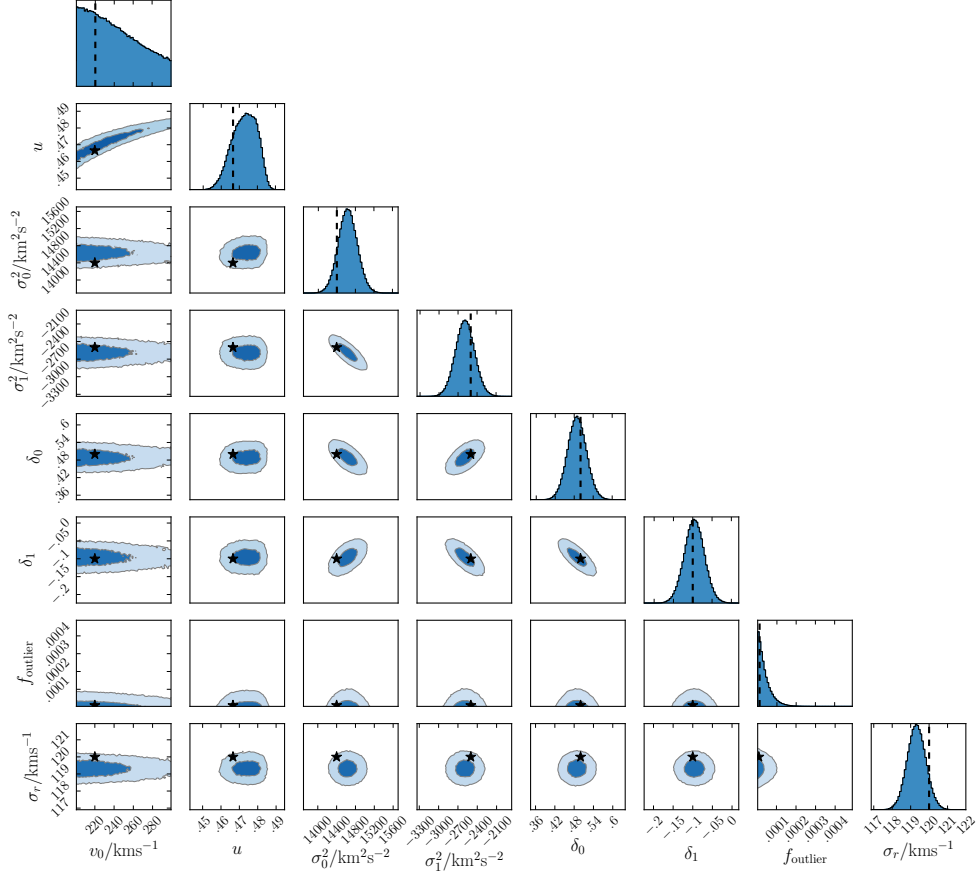


Figure 1. One and two dimensional marginalisations of the posterior probability distribution when our method is applied to a mock catalogue of ~ 24000 stars without uncertainties. True values are marked by dashed lines (black stars) in the one (two) dimensional distributions. The nuisance parameters are all well constrained without bias. The degeneracy between q and v_0 is apparent in the 2D marginalised distribution, though our prior on v_0 prevents the MCMC from sampling unrealistic circular speeds (and hence unrealistic values of q). The Gelman-Rubin statistic for this chain is $\simeq 1.002$.

In principle, there are six components of the velocity dispersion tensor, but only three Jeans equations. However, if the alignment of the velocity ellipsoid is known, this reduces to three equations for the three unknown principal components. Here, we can exploit the fact that the velocity ellipsoid of halo stars is closely aligned with the spherical polar coordinate system with all the misalignment angles small (Smith et al. 2009a; Bond et al. 2010; Evans et al. 2016; King et al. 2015). Spherically aligned solutions of the Jeans equations have received little attention, despite early work by Bacon et al. (1983) and Bacon (1985). In Section 2, we derive the angular Jeans equation – or *the flattening equation* – under the assumption of spherical alignment. This relates the shape of the dark halo to the angular velocity dispersions and the gradients in the stellar density. Then, in Section 3, we devise a numerical algorithm to solve the flattening equation and construct the likelihood. Section 4 shows tests of the procedure with mock data, together with application to the dataset of Bond et al. (2010) to deduce the

shape of the Milky Way’s dark halo. We discuss our results, and compare to other recent work, in Section 5.

2 THE FLATTENING EQUATION

In an axisymmetric model, $\langle v_r v_\phi \rangle \equiv \langle v_\theta v_\phi \rangle \equiv 0$ by the symmetries of the individual orbits, which then leaves two non-trivial Jeans equations for the tracer density $\nu(r, \theta)$ in terms of the potential $\Phi(r, \theta)$:

$$\frac{\partial \nu \langle v_r^2 \rangle}{\partial r} + \frac{1}{r} \frac{\partial \nu \langle v_r v_\theta \rangle}{\partial \theta} + \frac{\nu}{r} \left(2 \langle v_r^2 \rangle - \langle v_\theta^2 \rangle - \langle v_\phi^2 \rangle + \langle v_r v_\theta \rangle \cot \theta \right) = \nu \frac{\partial \Phi}{\partial r} \quad (1)$$

$$\frac{\partial \nu \langle v_r v_\theta \rangle}{\partial r} + \frac{1}{r} \frac{\partial \nu \langle v_\theta^2 \rangle}{\partial \theta} + \frac{\nu}{r} \left[3 \langle v_r v_\theta \rangle + (\langle v_\theta^2 \rangle - \langle v_\phi^2 \rangle) \cot \theta \right] = \frac{\nu}{r} \frac{\partial \Phi}{\partial \theta}. \quad (2)$$

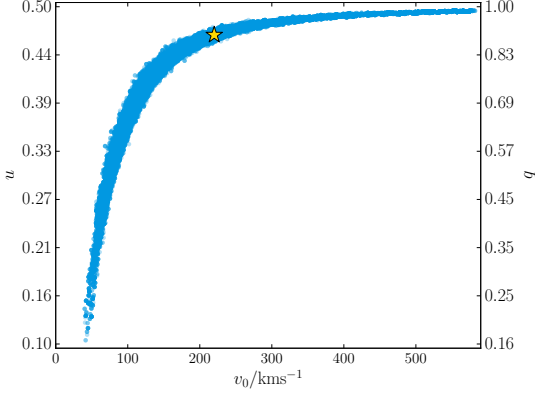


Figure 2. Illustration of the degeneracy between the flattening q (or u) and velocity normalisation v_0 . We fix all model parameters to their input values except for the potential parameters, and then sample the remaining 2–dimensional space with EMCEE. The input potential parameters are marked with a star. The posterior is almost constant along the centre of the degeneracy – our method is unable to precisely constrain q without prior knowledge of the normalisation of the potential.

These two relations between the four stresses $\rho\langle v_r^2 \rangle$, $\rho\langle v_r v_\theta \rangle$, $\rho\langle v_\theta^2 \rangle$, $\rho\langle v_\phi^2 \rangle$ must be satisfied everywhere. We specialize immediately to spherical alignment, $\langle v_r v_\theta \rangle = 0$, as it holds good for the Milky Way’s stellar halo (e.g., Evans et al. 2016, and references therein). This leaves two equations for three unknowns $\langle v_r^2 \rangle$, $\langle v_\theta^2 \rangle$ and $\langle v_\phi^2 \rangle$, if the density and potential are given. The first is the familiar radial Jeans equation:

$$\frac{\partial \nu \langle v_r^2 \rangle}{\partial r} + \frac{\nu}{r} (2\langle v_r^2 \rangle - \langle v_\theta^2 \rangle - \langle v_\phi^2 \rangle) = \nu \frac{\partial \Phi}{\partial r}. \quad (3)$$

This equation is usually recast in a slightly different form, by prescribing an anisotropy parameter $\beta(r)$ defined as $\beta(r) = 1 - (\langle v_\theta^2 \rangle + \langle v_\phi^2 \rangle) / 2\langle v_r^2 \rangle$. Now the Jeans equation can be easily solved using the integrating factor, as noted before many times (e.g., van der Marel 1994; Mamon & Lokas 2005; Evans & An 2006; Agnello et al. 2014).

The second is the angular Jeans equation, or *the flattening equation*:

$$\frac{\partial \nu \langle v_\theta^2 \rangle}{\partial \theta} + \nu (\langle v_\theta^2 \rangle - \langle v_\phi^2 \rangle) \cot \theta = \nu \frac{\partial \Phi}{\partial \theta}. \quad (4)$$

The sign of the right-hand side of the equation is controlled by the flattening of the gravity field, and is positive, zero or negative according to whether the total matter distribution is oblate, spherical or prolate. For the Milky Way galaxy, the first term on the left hand-side contains contributions from the angular gradient in stellar density $\partial \nu / \partial \theta$. As the stellar halo is oblate, this contribution is positive and drives the solution to oblateness. However, the contribution from the angular gradient of $\partial \langle v_\theta^2 \rangle / \partial \theta$ is negative and has the converse effect. Finally, the second term on the left-hand side is small as $\langle v_\theta^2 \rangle \gtrsim \langle v_\phi^2 \rangle$. It is usually negative (though not always, see e.g., Table 1 of Evans et al 2015) and so drives the solution to prolateness. The result of the competing effects of these terms gives the flattening as a function of radius. Now notice something else that is simple, but crucial. The flattening equation does not involve the radial velocity dispersion at all. In spherical alignment, the flattening of the potential is independent of both radial gradients and the radial

velocity dispersion. This decoupling considerably simplifies the solutions of the axisymmetric Jeans equations.

First, though, we have to provide an analogue of the anisotropy parameter $\beta(r)$ that prescribes how the angular velocity dispersions are related. We must have $\langle v_\theta^2 \rangle = \langle v_\phi^2 \rangle$ on the pole $\theta = 0$ on symmetry grounds. It has long been known that, away from the pole, $\langle v_\theta^2 \rangle \gtrsim \langle v_\phi^2 \rangle$ for the stellar halo (see e.g., Kepley et al. 2007; Smith et al. 2009b; Bond et al. 2010). Without loss of generality, the angular variation in the difference between $\langle v_\theta^2 \rangle$ and $\langle v_\phi^2 \rangle$ can be expanded in an even Fourier series

$$1 - \frac{\langle v_\phi^2 \rangle}{\langle v_\theta^2 \rangle} = - \sum_{m=1}^{\infty} \Delta_m \sin^{2m} \theta, \quad (5)$$

where Δ_m may depend on r but not on θ . This naturally satisfies the constraint on the pole. Then, the flattening equation is solvable with an integrating factor

$$j(\theta) = \prod_m \exp \left(- \frac{\Delta_m}{2m} \sin^{2m} \theta \right). \quad (6)$$

If boundary conditions are given on the conical surface $\theta = \theta_0$, then the full solution is

$$\nu \langle v_\theta^2 \rangle = \frac{1}{j(\theta)} \left[j(\theta_0) \nu \langle v_\theta^2 \rangle \right]_{r, \theta_0} + \int_{\theta_0}^{\theta} d\theta' j(\theta') \nu(r, \theta') \frac{\partial \Phi}{\partial \theta'}. \quad (7)$$

This gives both $\langle v_\theta^2 \rangle$ and $\langle v_\phi^2 \rangle$ everywhere as single quadratures.

Solutions of the Jeans equations for spherical alignment have been given before (Bacon et al. 1983; Bacon 1985; Evans et al. 1997). The advantage of the algorithm presented here is that it provides a practical parametrisation that enables physically motivated solutions to the flattening equation to be constructed very easily. As always with solutions of the Jeans equations, there is no guarantee that there exists an underlying positive-definite solution for the phase space distribution function. In fact, Evans et al. (2016) and An & Evans (2016) have shown that exact spherical alignment of the second velocity moments implies that the potential is separable or Stäckel. Nevertheless, even mild misalignments allow a much greater range of possible equilibria, as Evans et al. (2016) demonstrated with made-to-measure N-body techniques. It is reasonable to expect some, perhaps many, of our spherically aligned Jeans solutions do therefore correspond to physical equilibria.

3 NUMERICAL IMPLEMENTATION

3.1 Data

We now describe the data set which we wish to model in a little more detail. Loebman et al. (2014) extract halo stars from the SDSS data by cutting in colour $0.2 < g - r < 0.6$ and in metallicity $[\text{Fe}/\text{H}] < -1.1$. There is some contamination from the disk populations, which is estimated at ~ 6 per cent (Loebman et al. 2014). To further reduce disk contamination, we remove all stars with $|z| < 2$ kpc.

We choose to focus on a subsample extending over Galactocentric spherical polar radii $5 \lesssim r \lesssim 10$ kpc. Requiring the stars possess SDSS spectra for radial velocities

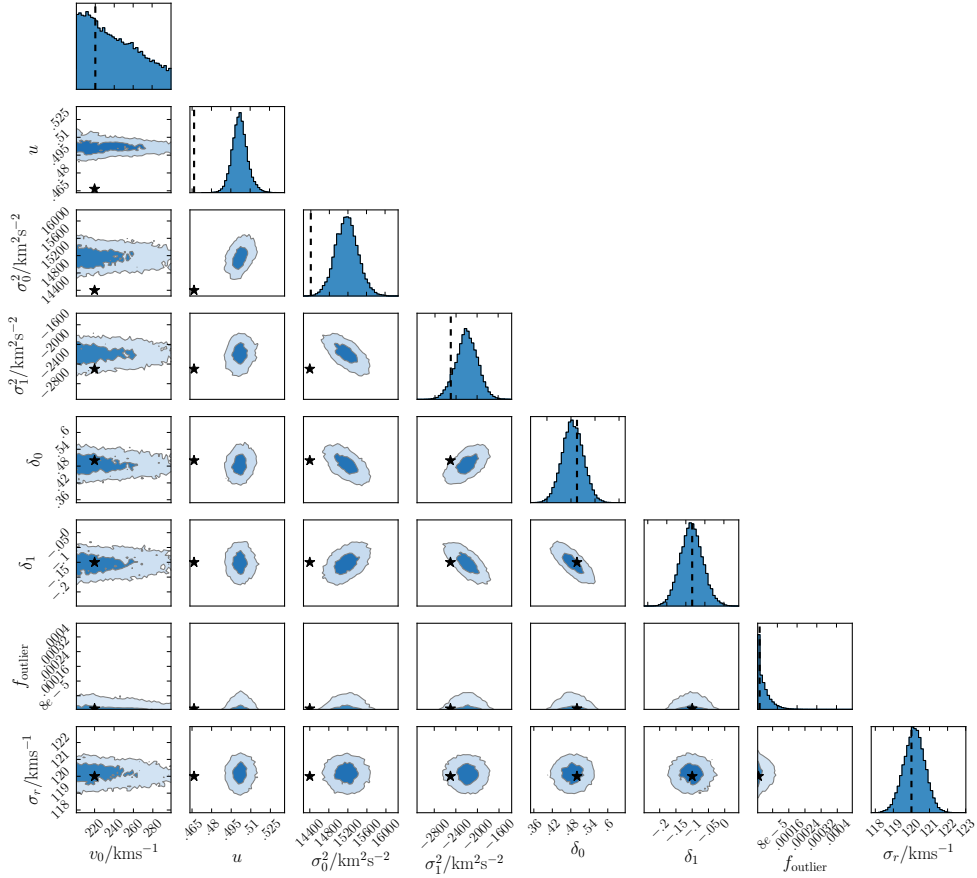


Figure 3. As Fig. 1, but now using a mock catalogue of ~ 24000 stars incorporating uncertainties typical of the Bond et al. (2010) data. The observational errors can scatter the value of the flattening away from the correct answer ($q = 0.9$ or $u = 0.467$) to more spherical models. This is due to Poisson noise, which remains a problem despite the size of dataset.

and POSS astrometry for proper motions yields a large sample of 14853 halo stars. We use the errors on the velocities computed by the SDSS pipeline, and ignore any possible systematic effects. The SDSS pipeline also provides photometric errors, which can be used to compute random errors in absolute magnitude (assuming that the covariances between bands are negligible). Polynomial relations for the absolute magnitude of F and G stars as a function of g , r , i and metallicity $[\text{Fe}/\text{H}]$ are given in Ivezić et al. (2008).

3.2 Numerical Solution

A significant defect of many solutions of the Jeans equations presented in the literature is that the boundary conditions are often applied at infinity. This requires assumptions as to the form of the gravitational potential and density well beyond the limits of the data, and so is unattractive. We eschew this practice and integrate forwards and backwards from a cone embedded within the data, using the data itself to set the boundary conditions.

We parameterize the angular velocity dispersion on the

conical surface $\theta = \theta_0$ as

$$\langle v_\theta^2 \rangle = \sum_m \sigma_m^2 \left(\frac{r - r_d}{\delta r} \right)^m = \sigma_d^2(r), \quad (8)$$

where $r_d = 7.5$ kpc is a characteristic radius of the stars in our sample and $\delta r = 2.5$ kpc is characteristic of the distance range our data covers. This is of course a Taylor series about $r = r_d$. We find that taking six terms of this series works well in our application for which the data are restricted to spherical polar radii in the range $5 \lesssim r \lesssim 10$ kpc.

The solution for the angular velocity dispersion is obtained by integrating the flattening equation forwards or backwards:

$$\begin{aligned} \nu \langle v_\theta^2 \rangle &= \exp\left(\frac{\Delta}{2} \sin^2 \theta\right) \left[\exp\left(-\frac{\Delta}{2} \sin^2 \theta_0\right) \nu(r, \theta_0) \sigma_d^2(r) \right. \\ &\quad \left. + \int_{\theta_0}^{\theta} d\theta' \exp\left(-\frac{\Delta}{2} \sin^2 \theta'\right) \nu(r, \theta') \frac{\partial \Phi}{\partial \theta'} \right]. \quad (9) \end{aligned}$$

This is simpler than the full solution (7), as the quality of the present data set only warrants the use of the first term ($m = 1$) in the Fourier series (5). We have retained only

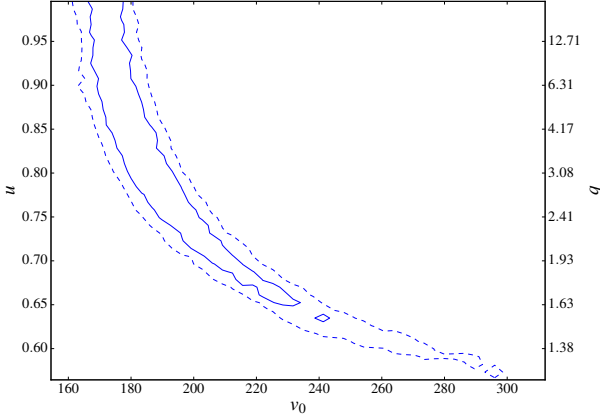


Figure 4. The two-dimensional posterior parameter distributions for velocity normalisation v_0 in kms^{-1} and halo flattening q (or u) of 140,000 samples for the converged Monte Carlo chain. We observe the expected degeneracy here, however for the range of plausible halo normalizations the shape remains distinctly prolate. The Gelman-Rubin statistic for this chain is $\simeq 1.004$.

this term and dropped the subscript on Δ_1 . Then, the physical meaning of Δ is that it is the maximum value of the angular anisotropy $\langle v_\theta^2 \rangle / \langle v_\phi^2 \rangle - 1$, which occurs on the equatorial plane $\theta = \pi/2$. Just as for the boundary condition, we use a Taylor series to describe the radial variation of the anisotropy parameter,

$$\Delta(r) = \sum_m \delta_m \left(\frac{r - r_d}{\delta r} \right)^m, \quad (10)$$

and usually take the first six terms of the series in our applications to data.

Solution of Eq. (9) also requires parameterization of the potential. We use a family of halo potentials of the form

$$\Phi = -v_0^2 \ln \left(R^2 + \frac{z^2}{q^2} \right), \quad (11)$$

where (R, z) are cylindrical polar coordinates. Although widely used (e.g. Evans 1993; Binney & Tremaine 2008; Bowden et al. 2015), it is unlikely that the Galactic potential is as simple as this. We have experimented with inclusion of a baryonic disk, but we find that this make little difference to our conclusions on the flattening. This is less surprising on recalling that we are primarily interested in determining whether the halo is oblate ($q < 1$) or prolate ($q > 1$), and less concerned about the specific value of q .

3.3 Likelihood Construction

We implement a full Bayesian analysis of the data. The data form a vector of observables $\mathbf{L} = (s, \ell, b, v_{||}, \boldsymbol{\mu})$. Here, (s, ℓ, b) are heliocentric distance, Galactic longitude and latitude, while $(v_{||}, \boldsymbol{\mu})$, are line of sight velocity and proper motion. We must transform the likelihood function from observable space into spherical polars $(\mathbf{x}, \mathbf{v}) = (r, \theta, \phi, v_r, v_\theta, v_\phi)$. This is achieved via a Jacobian factor

$$p(\mathbf{L}|\mathcal{P}) = p(\mathbf{x}, \mathbf{v}|\mathcal{P}) \left| \frac{\partial(\mathbf{x}, \mathbf{v})}{\partial \mathbf{L}} \right|, \quad (12)$$

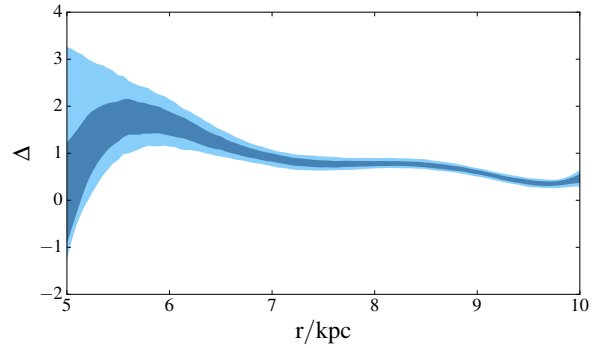
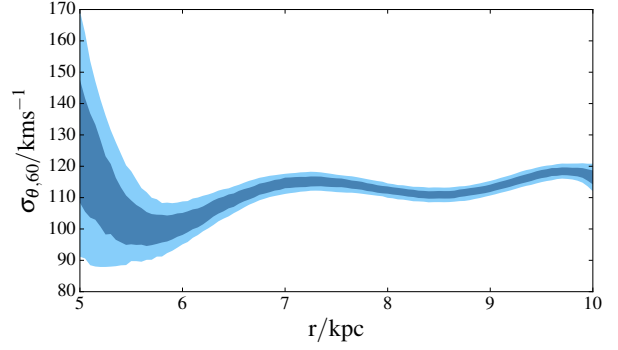


Figure 5. Plot showing an aggregation of posterior parameter distributions for 25,000 samples for the converged Monte Carlo chain. The dark blue shows 1σ contours containing 68.27% of the samples; the light blue shows 2σ , containing 95.45%. The left panel shows the boundary condition for our integration, the value of σ_θ^2 on the conical surface $\theta_0 = 60^\circ$. The right panel shows the angular anisotropy parameter Δ parameter, which relates the two components of the angular velocity dispersion.

where

$$\frac{\partial(\mathbf{x}, \mathbf{v})}{\partial \mathbf{L}} = \frac{s^4 \cos b}{r^2 \sin \theta}. \quad (13)$$

We now construct a model that is compatible with our solutions to the Jeans equations. Using the product rule for probabilities, we have

$$p(\mathbf{x}, \mathbf{v}|\mathcal{P}) = p(\mathbf{v}|\mathbf{x}, \mathcal{P}) p(\mathbf{x}|\mathcal{P}), \quad (14)$$

where $p(\mathbf{v}|\mathbf{x}, \mathcal{P})$ is the local velocity distribution and $p(\mathbf{x}|\mathcal{P})$ is proportional to the density law of the tracer, in our case the stellar halo. We take $p(\mathbf{x}|\mathcal{P}) = 2\pi r^2 \sin \theta \nu(r, \theta)$ where

$$\nu(r, \theta) \propto r^{-n_*} (\sin^2 \theta + \cos^2 \theta / q_*^2)^{-n_*/2} \quad (15)$$

with $q_* = 0.64$ and $n_* = 2.77$. This single power-law model was found by Jurić et al. (2008) to be a good match to SDSS main-sequence turn-off halo stars and is valid in the distance regime probed by the Bond et al. (2010) data. In our work, we take the density as fixed in the sense that we do not seek to constrain its parameters, but it would be simple

to incorporate into future work, provided that the survey selection function is known. We then assume that the local velocity distribution of halo stars is given by the product of three Gaussian distributions

$$p_{\text{halo}}(\mathbf{v}|\mathbf{x}, \mathcal{P}) = \mathcal{G}(v_r | 0, \sigma_r) \mathcal{G}(v_\theta | 0, \sigma_\theta(r, \theta)) \mathcal{G}(v_\phi | 0, \sigma_\phi(r, \theta)) \quad (16)$$

where we have introduced the shorthand

$$\mathcal{G}(v|\mu, \sigma) = \frac{1}{\sqrt{2\pi}\sigma} \exp\left(-\frac{(v-\mu)^2}{2\sigma^2}\right), \quad (17)$$

and $\sigma_\theta(r, \theta)$ and $\sigma_\phi(r, \theta)$ are the solutions for the velocity dispersions given the current set of parameters \mathcal{P} and the Jeans equations. Note that we are assuming that the stellar halo has no mean rotation (see e.g., Kepley et al. 2007; Smith et al. 2009b). This parameterization encodes our solutions to the Jeans equations, ensures spherical alignment of the velocity ellipsoid, and gives a plausible shape to the local velocity distributions.

For now, we make the crude assumption that the radial velocity dispersion is constant with position – this will not bias our inference, although it is a signal that we are neglecting further information that is encoded in the (spherical) radial velocities of the stars. It is evidently possible to also solve the radial Jeans equation, and thus introduce $\sigma_r(r, \theta)$, which would provide further information about the gravitational potential. We opt not to do this currently, since it involves the evaluation of a two-dimensional quadrature and is hence much more time-consuming. For the time being, we explore how much can be learned from consideration of only the tangential velocities. To account for outliers in the data, we add a further component to the velocity distribution given by

$$p_{\text{outlier}}(\mathbf{v}) = \prod_{i=r,\theta,\phi} \mathcal{G}(v_i | 0, 1000 \text{ km s}^{-1}) \quad (18)$$

so that the full local velocity distribution is

$$p(\mathbf{v}|\mathbf{x}, \mathcal{P}) = (1-f)p_{\text{halo}} + fp_{\text{outlier}}, \quad (19)$$

where f is the outlier fraction, which we leave as a free parameter.

Given the above discussion, the likelihood function for an individual datum with no observational errors is

$$p(\mathbf{L}|\mathcal{P}) = p(\mathbf{v}|\mathbf{x}, \mathcal{P}) 2\pi s^4 \nu(r, \theta) |\cos b|. \quad (20)$$

To incorporate observational errors into our model, we write

$$p(\mathbf{L}|\mathcal{P}) = \int d\mathbf{L}' p(\mathbf{L}|\mathbf{L}', \mathbf{C}) p(\mathbf{L}'|\mathcal{P}), \quad (21)$$

where $p(\mathbf{L}|\mathbf{L}', \mathbf{C})$ is the probability of observing the coordinates \mathbf{L} given some true coordinates \mathbf{L}' . We characterize this distribution as a multivariate Gaussian with covariance matrix \mathbf{C} . We further assume that \mathbf{C} is diagonal, so that there are no covariances between uncertainties on each of the observable coordinates. Eqn (21) cannot be evaluated analytically, and so we evaluate it using the principle of Monte-Carlo integration. As in Evans et al. (2016; see also McMillan & Binney 2013), we draw N samples from $p(\mathbf{L}|\mathbf{L}', \mathbf{C})$, and approximate eqn (21) by

$$p(\mathbf{L}|\mathcal{P}) \simeq \frac{1}{N} \sum_{i=1}^N p(\mathbf{L}'_i|\mathcal{P}), \quad (22)$$

where $p(\mathbf{L}'_i|\mathcal{P})$ is the RHS of eqn (20) evaluated for the i th draw from the error ellipsoid of the star. It is important to note that we use the *same* Monte-Carlo samples for each star for each new set of parameters \mathcal{P} , so that the likelihood is not dominated by random noise (McMillan & Binney 2013). This means that, in practice, some of the terms in our likelihood function become constant as a function of the parameters, so that eqn (20) can be written as

$$p(\mathbf{L}|\mathcal{P}) \propto p(\mathbf{v}|\mathbf{x}, \mathcal{P}). \quad (23)$$

Terms dependent only on the positions of the stars are not variable between likelihood evaluations, since we use fixed Monte Carlo samples and do not vary the density law of the stars. As usual, we then presume that all of our stars are independent observations, and so the full likelihood is the product of eqn (22) for all of the stars in our sample.

3.4 Prior and Posterior Distributions

For the circular velocity of the gravitational potential v_0 , we experimented with a number of different priors. For tests using mock data, we show that a restricted range for v_0 is necessary in order to perform inference on the flattening; consequently, we use a Jeffreys prior within the limits $200 < v_0/\text{kms}^{-1} < 300$.

For the axis ratio q , we first make the transformation

$$u = \frac{2}{\pi} \arctan q, \quad (24)$$

which maps the infinite domain $[0, \infty]$ to the domain $[0, 1]$. The case $u = 1/2$ maps to $q = 1$, so that oblate models correspond to the range $0 < u < 1/2$ and prolate models are defined by $1/2 < u < 1$. In the case of complete ignorance of the axis ratio of the halo, an appropriate prior on u is therefore uniform on the domain $0 < u < 1$. We then sample the parameter u , which has a finite range. For the nuisance parameters, namely the coefficients in Taylor expansions of the angular anisotropy $\Delta(r)$ and the boundary condition on $\sigma_\theta^2(r, \theta = \pi/3)$, we assign priors that are uniform in regimes where the full functions satisfy

$$\begin{aligned} -4 &< \Delta(r) < 4, \\ 10^2 &< \sigma_\theta^2(r, \theta = \pi/3)/\text{km}^2\text{s}^{-2} < 700^2, \end{aligned} \quad (25)$$

for $5 < r/\text{kpc} < 10$. The prior on the outlier fraction f is uniform on the interval $0 < f < 1$. Later, we shall experiment with other priors, in particular on the velocity normalization of the gravitational potential. Given our priors, the full posterior probability for our model is then given by Bayes' theorem

$$p(\mathcal{P}|\mathcal{D}) = \frac{p(\mathcal{D}|\mathcal{P})p(\mathcal{P})}{p(\mathcal{D})}, \quad (26)$$

where $p(\mathcal{D}|\mathcal{P})$ is the product of eqn (22) for all of the stars in our sample and $p(\mathcal{P})$ are the prior distributions discussed in this section.

4 APPLICATIONS

4.1 Tests on Mock Data

To analyze the constraining power of our model, we now present tests on mock catalogues of stars drawn from our

model. Since we are assuming perfect knowledge of the tracer density, the precise positions of the stars in our mock catalogues are not important. All that we require is that the same density law is used to solve the Jeans equations as appears in eqn (20). To draw a mock sample, we use the following procedure:

- (i) Select parameters \mathcal{P} for the model, including all nuisance parameters.
- (ii) At the position (as implied by the reported distance) of each star in our SDSS sample, solve the Jeans equations given \mathcal{P} for $\sigma_\theta(r_i, \theta_i)$, $\sigma_\phi(r_i, \theta_i)$.
- (iii) For each star, draw each velocity v_j ($j = r, \theta, \phi$) from Gaussian distributions with $\mu = 0$ and $\sigma = \sigma_j(r_i, \theta_i)$. In the radial case, σ_r is a single parameter and independent of position.
- (iv) For each star we now possess $(\mathbf{x}_i, \mathbf{v}_i) = (r_i, \theta_i, \phi_i, v_{r,i}, v_{\theta,i}, v_{\phi,i})$. Convert these coordinates into $\mathbf{L} = (s_i, l_i, b_i, v_{||,i}, \boldsymbol{\mu}_i)$.
- (v) If scattering through some set of uncertainties $\boldsymbol{\delta} = (\delta_s, \delta_v, \delta_\mu)$, then for each star draw a new distance, line-of-sight velocity and set of proper motions from Gaussian distributions, e.g. $s'_i \sim \mathcal{G}(s_i, \delta_s)$.

Using the above prior probability distributions and likelihood, the results for a sample of comparable size to the SDSS data but without errors are shown in Fig. 1. We use two terms in each of the Taylor expansions of eqns (8) and (10). We do not include any outliers in our tests. The nuisance parameters are all well constrained. There is a noticeable degeneracy, however, between the potential parameters.

The degeneracy between v_0 and q is made explicit in Fig. 2. To produce the figure, we fixed all the nuisance parameters to their correct values, and then explored the remaining two-dimensional space with EMCEE, using the same mock data set as in Fig. 1. The degeneracy is narrow and very curved. Small circular speeds correspond to extremely oblate axis ratios, and larger circular speeds correspond to nearly spherical potentials. When the halo is prolate, the degeneracy looks much the same, except reflected about $q = 1$ and $q \rightarrow \infty$ when $v_0 \rightarrow 0$. This degeneracy arises because the flattening equation only deals with the angular derivative of the potential. As a result, any solution is invariant under the transformation $\Phi(r, \theta) \rightarrow \Phi(r, \theta) + F(r)$, where $F(r)$ is arbitrary. One way to break this degeneracy would be to consider the radial Jeans equation, which includes a term involving the radial derivative of the potential. However, as we have mentioned previously, this comes at a large computational cost. Fortunately, at plausible values of the circular speed ($v_0 > 200 \text{ km s}^{-1}$), the degeneracy is quite flat as a function of v_0 . In other words, v_0 is not well constrained, but q is. This is our reasoning for using a prior that limits v_0 to lie in the range $200 < v_0 / \text{kms}^{-1} < 300$. Once this prior is used, we recover the axis ratio of the potential reasonably well.

When we use error-free data and fix all of the parameters except q to their correct values, then there remains a range of ~ 0.05 in the maximum posterior value of q across 10 Monte Carlo samples. So, our results remain susceptible to Poisson noise despite the large sample size. When the observational errors are included, the results are shown in Fig. 3. Again, a sample of similar size to the SDSS data is used, together with the error distributions quoted by Bond

et al. (2010). Now, the posterior distribution of the flattening peaks close to spherical ($q = 1$ or $u = 0.5$) rather than at the oblate model ($q = 0.9$ or $u = 0.467$) used to generate the mock data. This effect is again a manifestation of Poisson noise, and may cause models that are close to spherical to be misclassified in terms of prolateness or oblateness.

Our results suggest that the flattening equation returns some useful, but limited, information given the data – we can say with reasonable confidence whether the potential is oblate or prolate, but not the degree to which this is the case, unless we use an informative prior on the potential normalization. Errors may cause mildly oblate or prolate models to be misclassified, but this applies at most to the range given by $0.9 \lesssim q \lesssim 1.1$, as judged from our experimentation.

4.2 Results

With the insights gained from mock catalogues, we now turn to the data. We use the Bayesian method described above with the simple two parameter halo consisting of a normalization v_0 and flattening q , as given in eq (11). We use a uniform prior on v_0 and a uniform prior on u defined in eq (24). There are thirteen further nuisance parameters – six Taylor series terms giving the boundary conditions for σ_θ on a conical surface, six Taylor series terms describing the relationship between σ_θ and σ_ϕ , and one for σ_r . We used a uniform prior on each of these parameters and assume no outliers in this case.

Fig. 4 shows the two-dimensional posterior parameter distribution for $\sim 140,000$ samples from a converged Monte Carlo chain. We give the full one-dimensional posteriors for the velocity normalization, flattening and all the nuisance parameters in Appendix A. We also performed the same fit with the inclusion of both a halo and a razor-thin exponential disk. The disk had a central surface density of $\Sigma_0 = 1.02 \times 10^9 \text{ M}_\odot \text{ kpc}^{-2}$ and a scalelength $R_d = 2.4 \text{ kpc}$ (c.f. Binney 2012). We verified that the presence of a baryonic disk component has minimal influence on the solution to the flattening equation in the region where we have data.

Although the data are not sufficient to constrain the halo flattening precisely, we see that prolate haloes (i.e., $u > 1/2$) are strongly favoured, with the posteriors ranging from near spherical to very strongly prolate. The flattening equation offers a robust determination of the gross shape, as oblateness or prolateness correspond to different signs of the left-hand side of eqn (4). However, the actual constraint on the numerical value of q is weak. Stronger constraints could be obtained by simultaneously solving both the flattening equation and the radial Jeans equation (3), but the computational cost is punitive. Stronger constraints could also be obtained with more informative priors on v_0 , similar to the ones used in the tests on mock data. Specifically, if the velocity normalisation v_0 lies between 210 and 250 km s^{-1} (as seems reasonable on other grounds), then Fig. 4 implies that the axis ratio of the equipotentials q satisfies $1.5 \lesssim q \lesssim 2$. So, our principal conclusion of prolateness does not change. In Fig. 5, we also show the constraints on both the angular velocity dispersion on a conical surface $\theta_0 = 60^\circ$ above the plane and the angular anisotropy parameter Δ , which is positive implying $\langle v_\phi^2 \rangle > \langle v_\theta^2 \rangle$. These two parameters can be inferred directly from the data.

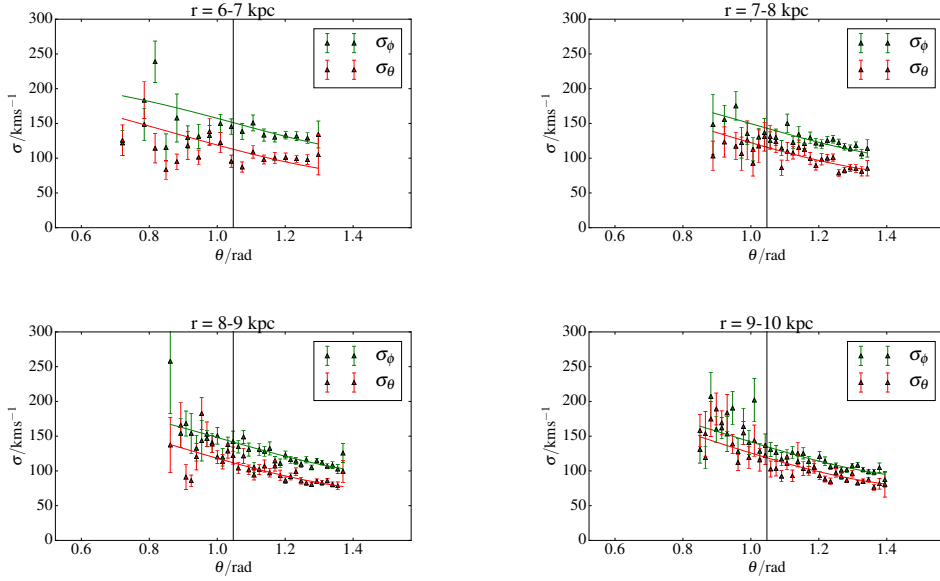


Figure 6. Sample fit for the binning method, showing the quality of the fit for the central three radial bins, namely 6-7 kpc (top left), 7-8 kpc (top right), 8-9 kpc (bottom left) and 9-10 kpc (bottom right). Green shows the σ_ϕ component, red the σ_θ . The vertical black line is marks the location $\theta_0 = 60^\circ$ where we set the boundary conditions for integration of the flattening equation.

We can perform an alternative test of the quality of our fits using a simple binning method. We divide our sample of stars into 2-D bins in r, θ . For each bin, we can evaluate σ_i^2 along with its error and use the likelihood function

$$\ln \mathcal{L} = -\frac{\chi^2}{2} = -\sum_m \frac{(\sigma_{\text{model},m}^2 - \sigma_{i,m}^2)^2}{2\epsilon_{i,m}^2}, \quad (27)$$

where $\epsilon_{i,m}^2$ denotes the error in σ_i^2 in bin m .

In practice, the radial range $5 \leq r \leq 10$ is divided into 1 kpc bins. The angular bins are chosen using the algorithm of Knuth (2006), with bins containing less than 10 stars removed. We find the results are consistent with the probabilistic method. As the binning method requires that we only draw once from the observational errors for each star, we repeated the fits with a number of different random seeds. Whilst there is a small amount of variation in the recovered parameters, the results are broadly consistent at the 1σ level. Fig. 6 shows an example fit from the final chain in the three central bins for the full probabilistic method; we see that the model provides a reasonable fit to the data in all four bins. The reduced χ^2 is 1.09 for this fit.

5 DISCUSSION AND CONCLUSIONS

The flattening equation robustly suggests that the shape of the Milky Way’s dark halo is prolate. Flattened oblate dark halos are strongly disfavoured. These statements hold true in the inner halo over the range of Galactocentric radii $5 \lesssim r \lesssim 10$ kpc. If we believe the halo is well represented by an axisymmetric logarithmic potential with velocity normalisation v_0 between 210 and 250 kms^{-1} , then the flattening equation implies that the axis ratio of the equipotentials q satisfies $1.5 \lesssim q \lesssim 2$. This result is consistent with the claim

of Banerjee & Jog (2011), who argued for prolateness based on an analysis of the HI flaring gas layer from 8 to 24 kpc.

However, the result is at variance with the work of Loebman et al. (2014), who analyzed the same data of Bond et al. (2010). Loebman et al. (2014) used the Jeans equations in a novel way to generate two dimensional acceleration maps from the data and then fit to galaxy models. This has the advantage that boundary conditions do not have to be prescribed, but it has the disadvantage that spatial gradients of the density and the components of the velocity dispersion tensor have to be evaluated from noisy data. They came to the conclusion that the dark halo is highly oblate with $b/a \approx 0.4 \pm 0.1$. Curiously, this is flatter than the stellar halo itself, which has an axis ratio $b/a \approx 0.6$ (e.g., Jurić et al. 2008; Watkins et al. 2009; Deason et al. 2011; Pila-Díez et al. 2015). As the dark matter is dissipationless whereas the baryons are not, it is more natural to expect that the dark halo is rounder than the stellar halo.

The flattening equation is a robust way to assess the oblateness or prolateness of the dark halo. Although there is a strong degeneracy between circular speed and flattening, we have shown that informative priors on the circular speed enable the flattening to be recovered, albeit with a mild bias when the data are scattered by the observational errors. Therefore, we advocate the use of the flattening equation to test for oblateness or prolateness, but not to measure the precise value of q . If that is desired, the flattening equation must be coupled with the radial Jeans equation in a computationally efficient algorithm for large datasets. This work is under investigation.

The only assumption in the method is spherical alignment of the velocity ellipsoid, which has been confirmed by several independent studies (Smith et al. 2009a; Bond et al. 2010; Evans et al. 2016; King et al. 2015). Other than

three dimensional velocity data, the main ingredient needed is the stellar halo density law. This has also been measured by a number of workers (see e.g., Table 6 of Pila-Díez et al. 2015) with increasing consistency of results. Although we used the law advocated by Jurić et al. (2008) here, we have verified that different profiles (e.g., Deason et al. 2011) do not change the principal conclusion of prolateness.

Other arguments have been advanced against oblate halos, of which the most durable is the orbit of the Sagittarius stream. It would be improper to suggest that this puzzling object is well understood, but the conclusion that the orbit is inconsistent with oblate haloes has persisted despite a wealth of new data and modelling (Ibata et al. 2001; Evans & Bowden 2014). In fact, Helmi (2004) already claimed from analysis of the velocities of stars in the leading arm at ~ 40 kpc that the halo is prolate. However, the stellar kinematical analysis in this paper is confined mainly to the inner halo, whereas the Sagittarius stream is a gigantic object with debris extending from radii of 20 kpc to 100 kpc.

Of course, the coming of the first data sets from the *Gaia* satellite will revolutionise this activity with abundant proper motion data for halo stars brighter than $V \approx 20$. The flattening equation will then provide a computationally efficient way of mapping the halo shape as a function of Galactocentric radius using the space velocities and errors of individual stars. This may finally resolve the controversy of the shape of the Milky Way halo.

ACKNOWLEDGMENTS

We thank the anonymous referee for a thoughtful criticism of the first version of this paper. ADB and AAW thank the Science and Technology Facilities Council (STFC) of the United Kingdom for financial support.

REFERENCES

- An, J. H., Evans, N. W. 2016, ApJ, 816, 35
 Agnello, A., Evans, N. W., Romanowsky, A. J. 2014, MNRAS, 442, 3284
 Bacon, R., Simien, F., Monnet, G. 1983, AA, 128, 405
 Bacon, R. 1985, AA, 143, 84
 Banerjee, A., & Jog, C. J. 2011, ApJ, 732, L8
 Binney, J. J., Davies, R. L., Illingworth, G. D. 1990, ApJ, 361, 78
 Binney, J., Tremaine, S. 2008, Galactic Dynamics, Princeton University Press, 2nd edition
 Binney, J. 2012, MNRAS, 426, 1328
 Bond N. A., Ivezić, Ž., Sesar B., et al. 2010, ApJ, 716, 1
 Bowden, A., Belokurov, V., Evans, N. W. 2015, MNRAS, 449, 1391
 Cappellari, M. 2008, MNRAS, 390, 71
 Deason, A. J., Belokurov, V., Evans, N. W. 2011, MNRAS, 416, 2903
 Evans, N.W., 1993, MNRAS, 260, 191
 Evans, N. W., An, J. H. 2006, Phys Rev D, 73, 023524
 Evans, N. W., Bowden, A. 2014, MNRAS, 443, 2
 Evans, N. W., Hafner R. M., de Zeeuw P. T. 1997, MNRAS, 286, 315
 Evans, N. W., Sanders J.L, Williams A.A., An J.H., Lynden-Bell D., Dehnen W. 2016, MNRAS, 456, 4506
 Fellhauer, M., Belokurov, V., Evans, N. W., et al. 2006, ApJ, 651, 167
 Foreman-Mackey, D., Hogg, D.W., Lang, D. & Goodman, J., PASP, 125, 306
 Helmi, A. 2004, ApJ, 610, L97
 Ibata, R., Lewis, G. F., Irwin, M., Totten, E., & Quinn, T. 2001, ApJ, 551, 294
 Ivezić Ž., Sesar B., Jurić M., et al. 2008, ApJ, 684, 287
 Jurić, M., Ivezić, Ž., Brooks, A., et al. 2008, ApJ, 673, 864
 Kepley A. A., et al. 2007, AJ, 134, 1579
 King III C., Brown W. R., Geller M. J., Kenyon S. J. 2015, arXiv:1506.05369
 Knuth, K. H. 2006, arXiv:physics/0605197
 Koposov, S. E., Rix, H.-W., & Hogg, D. W. 2010, ApJ, 712, 260
 Law, D. R., & Majewski, S. R. 2010, ApJ, 714, 229
 Loebman S. R., Ivezić Ž., Quinn T. R., et al. 2014, ApJ, 794, 151
 Mamon, G. A., Lokas, E. L. 2005, MNRAS, 363, 705
 McMillan, P. J., & Binney, J. J. 2013, MNRAS, 433, 1411
 Olling, R. P., & Merrifield, M. R. 2000, MNRAS, 311, 361
 Pila-Díez, B., de Jong, J. T. A., Kuijken, K., van der Burg, R. F. J., Hoekstra, H. 2015, A&A, 579, A38
 Schönrich R., Binney J., Dehnen W. 2010 MNRAS, 403, 1829
 Smith M. C., Evans N. W., An J. H. 2009a, ApJ, 698, 1110
 Smith M. C., Evans N. W., Belokurov V., et al. 2009b, MNRAS, 399, 1223
 van der Marel, R. P. 1994, MNRAS, 270, 271
 Vera-Ciro, C., & Helmi, A. 2013, ApJ, 773, L4
 Watkins, L. L., Evans, N. W., Belokurov, V., et al. 2009, MNRAS, 398, 1757

APPENDIX A: FULL POSTERiors

Here, for completeness, we give in Fig.7 the full posterior distributions on all the parameters for the final fit to the Bond et al. (2010) sample.

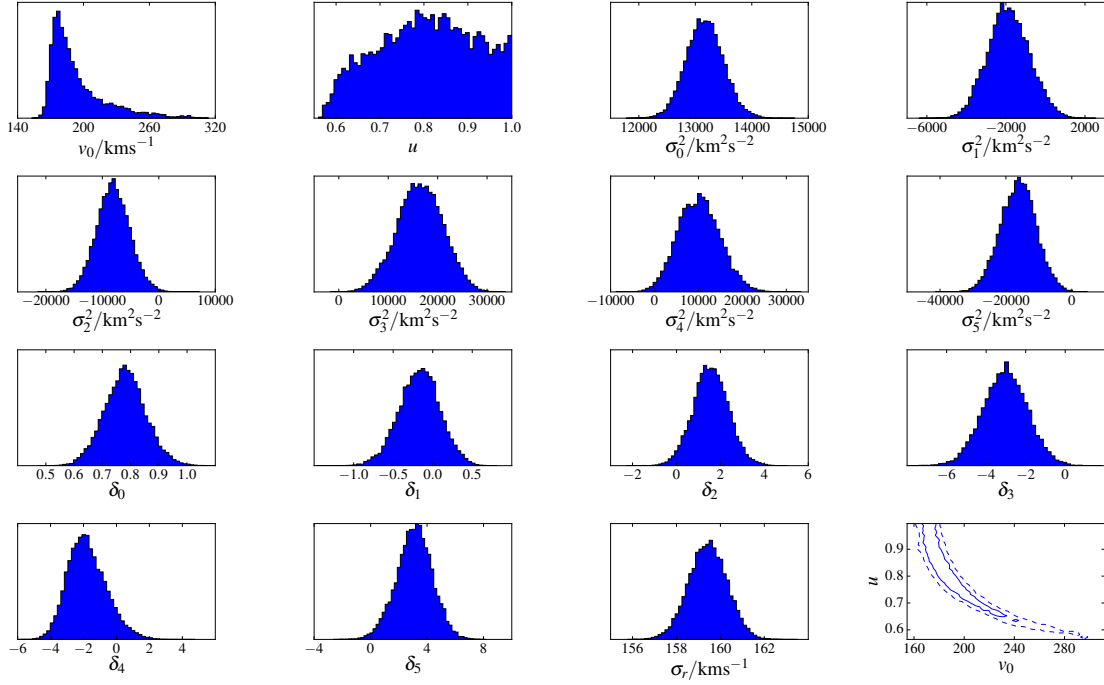


Figure 7. Plot showing the posterior parameter distributions of 140,000 samples for the converged Monte Carlo chain. The fitting was performed using the method described in Section 3, with a two parameter halo model (v_0, q). No baryonic disk component was included. The bottom right panel shows the two dimensional posterior for the halo parameters; we observe the expected degeneracy here, however even for realistic halo normalizations the shape remains distinctly prolate.